Molecular Cancer Therapeutics

A Murine Model for Quantitative, Real-Time Evaluation of Convection-Enhanced Delivery (RT-CED) Using an ^{18}[F]-Positron Emitting, Fluorescent Derivative of Dasatinib

Melinda Wang[1], Harikrishna Kommidi[2], Umberto Tosi[1], Hua Guo[2], Zhiping Zhou[3], Melanie E. Schweitzer[3], Linda Y. Wu[1], Ranjodh Singh[1], Shengqi Hou[4], Benedict Law[2], Richard Ting[2], and Mark M. Souweidane[3]

Abstract

The blood brain barrier can limit the efficacy of systemically delivered drugs in treating neurological malignancies; therefore, alternate routes of drug administration must be considered. The Abl-kinase inhibitor, dasatinib, is modified to give compound **1** ([^{18}F]-**1**) so that ^{18}F-positron emission tomography (PET) and fluorescent imaging can both be used to observe drug delivery to murine orthotopic glioma. *In vitro* Western blotting, binding studies (IC_{50} = 22 ± 5 nmol/L), and cell viability assays (IC_{50} = 46 ± 30 nmol/L) confirm nanomolar, *in vitro* effectiveness of [^{18}F]-**1**, a dasatinib derivative that is visible by ^{18}F-PET and fluorescence. [^{18}F]-**1** is used to image dynamic direct drug delivery via two different drug delivery techniques to orthotopic murine brainstem glioma (mBSG) bearing mice. Convection enhanced delivery (CED) delivers higher concentrations of drug to glioma-containing volumes versus systemic, tail-vein delivery. Accurate delivery and clearance data pertaining to dasatinib are observed, providing personalized information that is important in dosimetry and redosing. Cases of missed drug delivery are immediately recognized by PET/CT, allowing for prompt intervention in the case of missed delivery. *Mol Cancer Ther; 16(12); 2902–12. ©2017 AACR.*

Introduction

The blood brain barrier (BBB) limits our ability to utilize our full range of chemotherapeutics in brain cancer and may account for a lack of therapeutic benefit when *in vitro* strategies for primary glioma are brought to the clinic. Because of the BBB, many systemically delivered drugs demonstrating *in vitro* potential are unable to reach or maintain sufficient local concentrations in the central nervous system (CNS) to propagate a long-term therapeutic effect (1).

Convection-enhanced delivery (CED) bypasses the BBB to deliver chemotherapeutic agents directly to a target site at high-local concentrations that are difficult to achieve systemically (2). CED utilizes a pressure-driven infusion system to generate bulk flow, minimizing toxicity and enhancing the tumoral distribution of the delivered agent (3–5). CED is being investigated in diffuse intrinsic pontine glioma [DIPG, the United States and England (Trial identifier: NCT01502917)]. Because CED is new technique, a wide spectrum of standard effective parameters including infusate volume, rate of delivery, and region of injection are yet to be established. Unfortunately, CED is limited by an inability to quantitatively evaluate chemotherapeutic agent distribution. In the case that a cannula is dislodged or improperly placed during CED, a drug can be misdelivered. Without real-time imaging capabilities, symptoms of inaccurate drug delivery may be incorrectly interpreted as a lack of drug efficacy. One would only realize drug misdelivery by observing significant progression of disease (6), a delay that limits a patient's potential in other early, meaningful interventions.

In treating glioma and other CNS pathologies non-systemically, a means of accurately imaging drug delivery is needed. The current de facto clinical standard is gadolinium-based magnetic resonance imaging (MRI). Contrast surrogate agents, such as Gd-DTPA (Magnavist, Bayer; ref. 7), can be co-infused with a drug to mimic the distribution of therapeutic agents delivered by CED (8, 9). However, Gd-based contrast agents are not effective therapeutics on their own, and require micromolar quantities to resolve (10–12). Gd-DTPA cannot serve as a universal indicator of drug distribution as the diffusive properties of a drug are related to molecular size, mass, hydrogen bonding, and partition coefficient, properties that widely vary between drugs and tracers (8, 13, 14). Positron emission tomography (PET) can be more sensitive than MR contrast (8, 9, 15), making PET uniquely useful for tracking chemotherapeutics at nanomolar concentration. This is clear from recent efforts focused on ^{124}I-tagged antibodies, which have both a therapeutic effect in tumor-specific antigen targeting, and can be imaged by PET (3, 16, 17).

[1]Weill Cornell Medicine, New York, New York. [2]Molecular Imaging Innovations Institute (MI3), Department of Radiology, Weill Cornell Medicine, New York, New York. [3]Department of Neurological Surgery, Weill Cornell Medicine, New York, New York. [4]Department of Radiation Oncology, Weill Cornell Medicine, New York, New York.

Note: Supplementary data for this article are available at Molecular Cancer Therapeutics Online (http://mct.aacrjournals.org/).

M. Wang and H. Kommidi contributed equally to this article.

Corresponding Authors: Richard Ting, Weill Cornell Medicine, 413 East 69th Street, Box 290, New York, NY 10065. Phone: 646-962-6195; Fax: 646-962-0577; E-mail: rct2001@med.cornell.edu; and Mark M. Souweidane, Department of Neurological Surgery, Weill Cornell Medicine, 1300 York Avenue, New York, NY 10065. Phone: 212-746-2363; Fax: 212-746-7729; E-mail: mmsouwei@med.cornell.edu

doi: 10.1158/1535-7163.MCT-17-0423

PET is especially suited to drugs like the small molecule kinase inhibitor, dasatinib (Sprycel, Bristol Myers Squibb; refs. 18–20), which is effective at low, nanomolar concentrations. Many recognize this and report ^{18}F-labeled dasatinib derivatives for stand-alone PET imaging (19–21). In addition, dasatinib is of interest for the treatment of diffuse intrinsic pontine glioma (DIPG; refs. 5, 22). Dasatinib is also an ideal prototype for image-guided drug delivery because it can be diversely modified at its hydroxy terminal without detrimentally affecting its effectiveness as a drug (23).

To study drug delivery to the CNS via varying delivery systems, we modify dasatinib as an ^{18}F-PET agent (Fig. 1) and use it to evaluate CED-based intratumoral delivery and systemic intravenous delivery in orthotopic glioma murine models. We understand that the modification of any drug will cause its pharmaceutical properties to change substantially, especially when adding a large, charged fluorophore. We report a specific derivative of dasatinib that contributes only a minor perturbation to dasatinib *in vitro* IC_{50} and mechanism of action (~factor of 2, IC_{50}). We hypothesize that this agent could serve as a "proxy" for tracking the delivery and clearance of a small-molecule, anti-cancer therapeutic agent *in vivo* (as opposed to representing an exact, therapeutic equivalent of dasatinib itself). The resulting molecule is used to investigate the following *in vivo* hypotheses associated with CED: (i) that CED can safely and non-invasively deliver higher doses of a chemotherapeutic agent to glioma than is achievable in traditional intravenous delivery; (ii) that CED imaging data can be used to determine drug clearance, providing information for re-dosing; and (iii) that misdelivery can be immediately recognized through imaging.

Materials and Methods

Chemicals

The synthesis of compound **1** (Fig. 1A), a derivative of dasatinib for theranostic [$^{18/19}$F]-PET/FL imaging, is described in Fig. 1 (also see Supplementary Information). Compound **1** is stable, and fluoride loss is not observed in studies where **1** is stored in phosphate buffered saline (PBS)/fetal bovine serum (FBS; pH 7.4) for up to 7 days ($t_{1/2}$ defluoridation > 7 days measured by ^{19}F-NMR, see Supplementary Information; refs. 24, 25).

Cell lines

All cell lines were authenticated via PCR testing for adventitious viruses and mycoplasmas by the Weill Cornell Medicine Research Animal Resource Center (WCM RARC, September 2015). The efficacy of compound **1** was tested *in vitro* in a DIPG cell line generated from whole tumors of a PDGF-B driven and p53-deficient DIPG glioma derived from Nestin tv-a; p53 floxed mouse (26; received from Oren Becher, Duke University) and a murine brainstem glioma (mBSG) cell line. Cells were plated immediately after thawing and cultured in DMEM supplemented with 10% FBS and 100 μg/mL normocin and incubated at 37°C and 5% CO_2 and split approximately every 3 days.

Cellular viability assays and IC_{50} determination

Cells were plated in a 6-well plate with DMEM at a density of 50,000 cells/mL media and incubated for 24, 48, and 72 hours with 100 nmol/L of 1 in PBS. An untreated control, measured at 48 hours' postpassage, was performed. Commercial kits used for assaying cell viability include luminescent ATP detection assay (Promega, Cat# G7572), a cell-permeant calcein assay (Biotium, 30026), and a cell proliferation assay (Promega, Cat# G358C). The ATP-dependent luminescence assay was performed with the addition of 100 μL CellTiter Glo reagent into each well followed by incubation at room temperature for 15 minutes. Luminescence settings were used to collect data. For the Calcein AM assay, 100 μL of 4 μmol/L Calcein AM in PBS was added into each well. The mixture was incubated at 37°C for 30 minutes. Fluorescence was measured with an excitation wavelength of 485 and emission

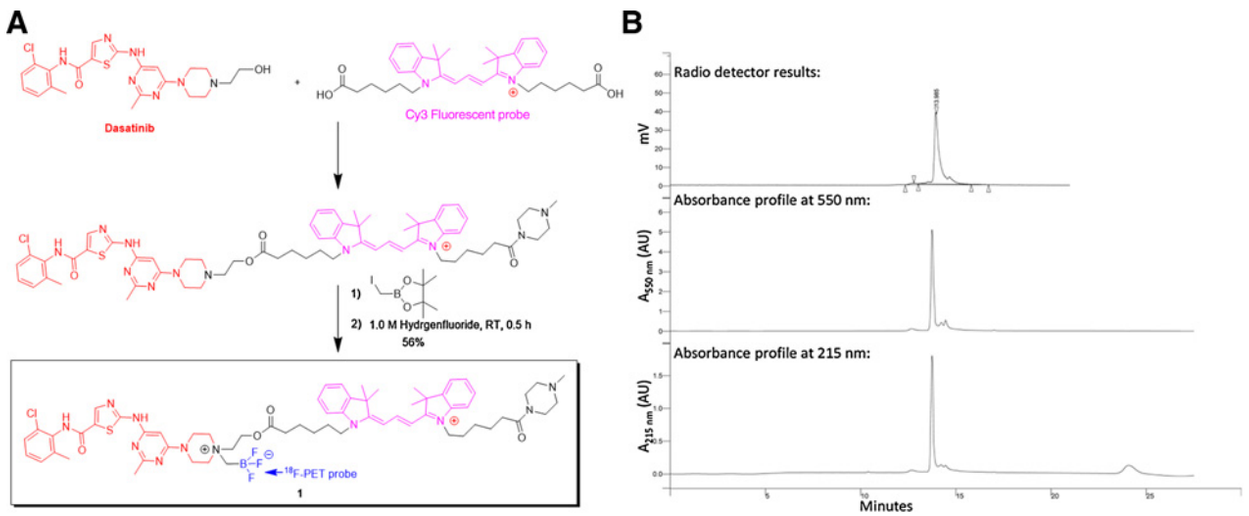

Figure 1.

Structure and characterization of compound **1**, ^{18}F-PET/FL labeled dasatinib for multimodality theranostic imaging. **A,** A scheme for synthesizing **1** from the commercial precursors dasatinib (red), N-methylpiperazine and trimethine cyanine (cy3, magenta). An ammoniomethyl trifluoroborate trap is used to capture positron emitting fluoride (blue). **B,** Reverse phase HPLC of [^{18}F]-**1** showing a pure radiosynthesis of **1** by scintillation, 550 nm, and 215 nm absorbance spectroscopy. In this preparation, 62% decay uncorrected radio chemical yield was achieved (35.8 mCi, 382 mCi/μmol synthesis in 25 minutes, from 86 mCi of activity).

filter at 530 nm. For the MTS cell proliferation assay, 20 μL of CellTiter 96 Aqueous One reagent was added into each well. The mixture was incubated at 37°C for 4 hours. Absorbance was measured at 490 nm. A Live/Dead C^{12} Resazurin, SYTOX Green cell viability assay (Thermo Fisher Scientific #L34951) was used to characterize percentage of cell death upon treatment. Flow cytometry was performed on a Gallios 1 Flow Cytometer.

Cells were plated in a 96-well plate with DMEM at a density of 5,000 cells/100 μL media and incubated for 48 hours with **1** or unmodified dasatinib. A 0.1% DMSO control was used. A [3-(4,5-dimethylthiazol-2-yl)-5-(3-carboxymethoxyphenyl)-2-(4-sulfophenyl)-2H-tetrazolium based cell proliferation assay (Promega Cat #G3580) was used per the manufacturer's protocol to characterize inhibition of cell proliferation and IC_{50}. Absorbance was read using Tecan Infinite M1000 Pro Microplate Reader at 490 nm. Independent, 3rd party verification of nanomolar activity was performed (LCK kinase profile assay, Nanosyn, Supplementary Fig. S1).

Fluorescence microscopy

Cells were plated on poly-D-lysine coated coverslips (NeuVitro H-12-pdl) and allowed to adhere overnight. Cells were stained with CellMask Deep Red plasma membrane stain (Thermo Fisher Scientific #C10046) by submerging in staining solution for 10 minutes at 37°C. After washing with PBS three times, 1 was added and allowed to incubate for 10 or 30 minutes. Three more washes with PBS were performed directly prior to imaging. Imaging was performed on an EVOS FL imaging system with 531(40)/593(40) nm ex/em filters.

[^{18}F]-Radiolabeling

[^{18}F]-fluoride-ion-containing water (500 μL) produced from a 15-minute, 19.2 MeV bombardment of [^{18}O]-water was flushed from a cyclotron target into a 5.0 mL glass v-vial (Thermo Scientific Reacti-Vial #13223). The vial was flushed with N_2 (28 ψ) at 100°C for 20 minutes through a 25G needle. To the resulting approximately 5 to 40 μl of concentrated, but not fully evaporated, aqueous volume (50–100 mCi of activity), a 0.2 mg (168 nmol) quantity of **1** was added and radiosynthesis was initiated with a 10 μl volume of 1 M pyridazine-HCl (pH = 2.0–2.5). The reaction was heated at 80°C for 17 minutes. Full solubility was observed on heating. 20 minutes later, the reaction was flushed with N_2 (28 ψ) at 80°C for 3 minutes to give a pink solid. The solid was resuspended with 1 mL of water, transferred to a 1.5 mL Eppendorf tube and centrifuged at 18,000 g for 1 minute. Water was decanted from the insoluble precipitate, which was washed three more times with water to remove contaminating [^{18}F]-fluoride ion. Reverse phase HPLC on a Phenomenex Luna C5 100 Å, 250 mm × 21.20 mm I.D. A 10-μm column (00A-4043-B0), with a 20 minute, a 10%–90% H_2O:ACN (0.05% TFA) gradient and a flow rate of 1 mL/minute confirm [^{18}F]-**1** radiolabeling (Fig. 1B). A pink solid containing 83 μg (70 nmol) and 35.8 mCi of [^{18}F]-**1** was obtained (382 mCi/μmol, 62% RCY, decay uncorrected values at 26 minutes vs. TOS; Fig. 1B).

Formulation for CED

A fraction of the isolated solid, 12.5 μg, 3.0 mCi of [^{18}F]-**1**, is fully solubilized with 110 μL of Ethanol and 110 μL of PBS, and passed through a 0.22-μm syringe filter. Aliquots (50/50 Ethanol/PBS 200, μL, 500 μCi) were drawn into U-100 insulin syringes, ready for intravenous injection or CED infusion. A pink colored, 50 μmol/L solution was obtained. Following CT scanning and the initiation of PET data collection, 6 μL volume (300 pmol) were infused into glioma bearing animals (17 minutes following start of PET). All mice survived CED infusion.

Animal studies

All procedures conducted in mice were approved by the Weill Cornell Medicine Institutional Animal Care and Use Committee (#2014-0030) and are consistent with the recommendations of the American Veterinary Medical Association and the National Institutes of Health Guide for the Care and Use of Laboratory Animals. This work is compliant with ARRIVE guidelines for how to report animal experiments. No Patient studies were conducted.

RCAS/tv-a mouse model of high-grade glioma

A total of 50 mice (26 M, 24 F; all between 4–5 weeks of age) underwent tumor induction. A RCAS/tv-a system was used to generate PDGF-B driven mouse models of high-grade glioma with p53-deficiency in Ntv-a mice of a C57BL6 background, as described by Hambardzumyan and colleagues (27). DF1 cells (virus producing cells) were cultured in DMEM supplemented with 10% FBS and 100 μg/mL Normocin and incubated at 39°C and 5% CO_2. Cells were transfected with RCAS-PDGF-B or RCAS-Cre and then used for injections after being passaged at least six times from the time of transfection. Animals were anesthetized with 2% isoflurane and then placed onto a stereotactic frame (Model 900; Kopf Instruments). The head was shaved and area prepped with povidone iodine and ethanol. A midline scalp incision (5 mm) was made, and the animal's skull was leveled using bregma and lambda as reference points. A 0.2-mm diameter burr hole was made at 0.5 mm anterior to bregma and 1.7 mm lateral to the right of midline. A 33-gauge blunt needle with a Nanofil syringe (World Precision Instruments) was used with a UMP-2 pump (World Precision Instruments) to target the striatum at a depth of 3.5 mm below the skill surface. One microliter of a 1:1 mixture of 4×10^4 DF1 cells expressing RCAS-PDGF-B and RCAS-Cre was injected into the right striatum of 4- to 6-week-old ntv-a; p53fl/fl mice to generate high-grade gliomas. All animals survived stereotaxic implantation of glioma-producing cells with minimal morbidity seen immediately postprocedure

Symptoms of tumorigenesis were apparent starting at 4 weeks postimplantation including weight loss, decreased activity, gait instability, and head tilt. Weight loss was tracked daily; when a single animal lost >10% of its prior weight, the animal was scanned on a 7.0 Tesla Preclinical MRI (Bruker) to confirm glioma burden, location, and size. Tumorigenesis was successful in a total of 40 of 48 mice (83%). Criteria for inclusion in further imaging studies included lack of hydrocephalus, and survival through the completion of PET/CT imaging totaling 5 hours. Only glioma that were between 2 and 4 mm in diameter were considered suitable for PET-CED imaging. Large glioma are lethal to mice, and, therefore, glioma greater than 4 mm in diameter were not generally observed. When experimental endpoints were reached, mice were euthanized. Brain tissue was resected and flash frozen. The extracted glioma was excised, frozen, and submitted for immunohistochemical staining (Supplementary Figs. S2 and S3; ref. 14).

Preparative surgery for CED

Animals were anesthetized with 2% isoflurane and placed on a Kopf 900 model stereotaxic frame. The head was shaved and area prepped with povidone iodine and ethanol. A midline incision (5 mm) was made to expose coronal and sagittal sutures. The animal's head was leveled within the stereotaxic frame using bregma and lambda as reference points. Using a dental drill, a 0.2 mm burr hole was made through the skull at 0.5 mm anterior and 1.7 mm lateral to bregma. A MR-compatible 26-gauge PEEK guide cannula with a 4-mm pedestal (C315GS-4-SP, Plastics One Inc) was secured onto the skull with medical grade UV-light cured adhesive (Star Technology) using 30-second irradiations from a hand-held UV black light (Taotronics) held 1 to 2 cm from the adhesive. Best results were achieved by securing the cannula directly onto the dry skull and using circumferential adhesive to prevent dislodgement of the cannula with movement from the animal. Surgery time is 30 minutes. All animals survived cannula placement ($n = 20$).

CED equipment and pump preparation

A microprocessor-controlled precision pump (Harvard Apparatus) was used at a rate of 0.1 μL/minute. MR-compatible 33-gauge PEEK internal cannulas (C15IS-4-SPC, Plastics One Inc.) customized to a needle length of 3.5 mm below pedestal were inserted through the guide cannulas and secured in place via a locking mechanism. The pump and cannula were connected using MR-compatible 0.027 × 0.045 polyvinylchloride (PVC) tubing (C12VT, Plastics One Inc.), secured in place with UV-light cured adhesive, allowing for the animals to receive CED infusions during imaging. Animals were then loaded into the Siemens Inveon PET/CET imaging platform. The bore of the PET/CT is calibrated at 21°C so an external heater was required to prevent mice from hypothermia. Some mice (<5%) did not survive until the end of the PET/CT scan due to hypothermia or prolonged anesthesia. These mice were not included in data processing. Dynamic PET/CT scanning data were acquired for 3 hours. (See Supplementary video S1 and S2 for video of successful CED implantation and delivery).

Distribution and clearance of modified dasatinib

Ntv-a; p53$^{fl/fl}$ glioma bearing mice were anesthetized with 2% isoflurane in oxygen and injected with the modified dasatinib either via CED or tail vein injection and imaged in a Siemens Inveon PET/CT imaging platform during and/or post infusion. A 10-minute CT scan was acquired before PET scanning was initiated. A 6-μL infusion (CED) at a rate of 0.1 μL/minute (60 minutes) of [^{18}F]-**1** was initiated during the PET scan (CED). A delay was introduced between the PET scan start and the start of CED to ensure capture of CED. Mice receiving [^{18}F]-**1** intravenously were injected with 6 μL of [^{18}F]-**1** through a tail vein immediately prior to a 10-minute CT. CT was immediately followed by a 3-hour PET scan. Following imaging, mice were sacrificed, the brains were resected, analyzed by fluorescence imaging, and placed in Tissue-Tek OCT. Compound (Sakura), flash frozen with liquid nitrogen and stored at −78°C in preparation for immunohistochemical analysis (Supplementary Figs. S2 and S3).

Long-term (30-day) postCED survival experiments

A 33-gauge blunt Nanofil syringe (World Precision Instruments) must be used instead of a Plastics One Inc. catheter (C315GS-4-SP) for CED delivery of [^{18}F]-**1** in survival experiments. Catheters must be removed following the CED experiment. If catheters are left implanted following CED, morbidity/mortality will result from attempts by mice to remove catheters. Mice were operated on and allowed to recover for 30 days postsurgery. No pathology was detected only normal brain anatomy was found, 30 days following CED (Supplementary Fig. S4). Edema, infiltration, or anatomical deformity were not detected. Observed behavior was normal. Weight fluctuated between 24.5 to 30 g, but did not decrease following surgery. Six animals were used in total ($n = 3$ CED with [^{18}F]-**1**, $n = 3$ sham surgery).

Data analysis and statistical methods

Fluorescent images were adjusted and analyzed using ImageJ. PET/CT dynamic reconstructions were performed on Siemen's Inveon Acquisition Workplace software. Reconstructed .hdr files were exported as DICOM files for PET/CT/MR alignment using open source Amide v1.0.4 software. Dynamic scanning was acquired according to a [^{11}C]-PET histogram protocol (10 frames × 3 seconds; followed by 5 × 30 seconds frames, 6 × 2 minutes, 5 × 5 minutes, 5 × 10 minutes, and 5 × 20 minutes). MR were used to guide the placement of 2 mm box-geometry, regions-of-interest (8 mm^3 ROI). Control ROI of identical geometry and volume were placed on the contralateral side of the brain (symmetrical to the glioma ROI vs. the sagittal suture). ROI were quantitated in Amide v1.0.4 to produce volume averaged values and error. A 2-mm cubic volume placed outside the mice was used as a control SUV volume, from which all other SUV values were corrected. An identical SUV volume was placed over the infusion site, where [^{18}F]-**1** is delivered at 50 μmol/L. Dynamic data were exported into excel to generate accumulation and clearance graphs. Plot errors were generated from regression analyses using Sigma Plot 10.

Results

The choice to modify any drug will cause its pharmaceutical properties to change substantially, especially upon conjugation to a large charged fluorophore. For this reason, any chemical modification of a drug, like dasatinib, must first be newly evaluated, *in vitro*, for activity and mechanism of action that are similar to the parent compound.

Justification of drug choice

The small-molecule dasatinib is an ideal prototype for CED-imaged guided drug delivery for three reasons: (i) dasatinib is of interest to pediatric neurosurgeons because of its utility in treating DIPG and other high-grade gliomas (5, 22); (ii) dasatinib is of interest to synthetic chemists because it bears piperazine and hydroxyl functionality that are uncomplicated to modify (see Supplementary Fig. S5); and (iii) dasatinib is of interest to medicinal chemists, as it is one of few small-molecule agents that can tolerate large chemical modifications without reducing nanomolar potential as demonstrated in published crystal (28) and structure-activity data (23, 29; see Supplementary Fig. S6). A LCK-kinase infused dasatinib structure (28) shows that dasatinib's hydroxy terminus is directed out of the active site, and is not involved in active-site recognition. A structure activity study shows that the hydroxy terminus of dasatinib can be covalently modified with reagents (23, 29) as large as a monoclonal antibody (23), without affecting its nanomolar effectiveness. Imaging (fluorescent) moieties are generally large and can introduce

significant molecular weight onto a conjugate, which can affect drug efficacy. Dasatinib is an exception, which is tolerant of fluorophore modifications (29). These data suggest that dasatinib is a good prototype for image guided drug delivery.

Chemical and radiochemical syntheses

[^{18}F]-PET labeled dasatinib, **1**, is a drug that is visible by both fluorescent and ^{18}F-PET imaging, and can be used to image drug distribution and clearance from glioma. **1** is ^{18}F-radiolabeled using aqueous, acid catalyzed ^{19}F-^{18}F isotopic exchange technology (30–33). This radiochemistry can be performed with minimal radiochemistry training ([^{18}F]-**1** is successfully generated in 100% of over 10 attempted radiolabelings). The ability to produce [^{18}F]-imaging agents infallibly was greatly appreciated in CED and orthotopic glioma imaging experiments. Cannula implantation surgeries are invasive and irreversible once initiated, and the survival window between observable symptoms of glioma maturity (MRI) and mortality/morbidity-requiring euthanasia is short (and variable, typically 3–7 days). Radiochemical yields and specific activities ranging from 12.3 ± 2.8 mCi and 373 ± 10 mCi/μmol were obtained (decay uncorrected).

The precursor, [^{19}F]-**1**, is non-radioactive and bears structure that is electronically identical to its radioactive ^{18}F counterpart. This allows [^{19}F]-**1** to be used *in-vitro*, without hazard, in the fluorescence-only mode in cellular assays (Supplementary Figs. S1, S4, S6, and S7–S10) and confirmative multimodality imaging (34).

In vitro, compound 1 has a nanomolar therapeutic potential

Compound **1** demonstrates a chemotherapeutic effect in target cells at nanomolar concentration. To show that [^{19}F]-**1** can act as a nanomolar, pharmacologic analogue of dasatinib, cell-cycle inhibition (Supplementary Fig. S7), cytotoxicity/cytostatic assays (Supplementary Fig. S8), cell proliferation assays (Supplementary Fig. S9), Western blots (Supplementary Fig. S10), and kinase binding studies (Supplementary Fig. S1) were performed *in vitro* to compare the effect and mechanism of action of [^{19}F]-**1** with dasatinib (Fig. 2).

In vitro, 1 inhibits cell proliferation at nanomolar concentration

In murine brainstem glioma (mBSG) cultures driven by PDGF-B overexpression and p53 loss, the administration of **1** at 100 nmol/L causes cell death in FACS Live/Dead viability assays (Fig. 2B). These results suggest that biologic activity is retained following modification for imaging. A percentage of cells undergo apoptosis in line with the mechanism of action of dasatinib (Supplementary Figs. S1, S6, S7–S10), which has been shown to be both cytostatic and cytotoxic *in vitro* (35, 36). In addition, the maximal effect on cell death is seen at 48 hours, with a smaller percentage of cell death at 72 hours (Fig. 2, Supplementary Figs. S8 and S9). This *in vitro* result is consistent with unmodified dasatinib, suggesting activation of alternative pathways resulting in development of molecular resistance (37).

The antagonist potency of [^{19}F]-**1** as evaluated on pontine glioma in ATP-dependent luminescent cell viability, cell-permeant calcein AM, and MTS cell proliferation assays is nanomolar in concentration, like that of unmodified dasatinib (Fig. 2C). The IC_{50}, of [^{19}F]-**1**, 46 ± 30 nmol/L, is similar but inferior to unmodified dasatinib 19 ± 20 nmol/L and derivatives (18, 19, 23), but more effective than doxorubicin (control) 710 ± 120 nmol/L. Having verified that the imaging modifications on [^{19}F]-**1** do not greatly alter effectiveness and mechanism of action *in vitro*, animal studies were conducted to evaluate *in vivo* CED distribution.

In vivo ^{18}F-PET imaging of CED delivery to orthotopic glioma

To distinguish drug resistance from drug misdelivery *in vivo*, a means of evaluating proper drug delivery is needed. Using [^{18}F]-**1**, dynamic PET is used to observe three qualities of CED drug delivery that are difficult to observe without imaging, including (i) the delivery of larger fractions of a drug to a solid glioma by CED versus systemic delivery, (ii) the quantification of drug clearance from the solid glioma, and (iii) the immediate recognition of incorrect or insufficient delivery to glioma.

Identifying orthotopic glioma maturity

A 7.0 Tesla Preclinical MRI (Bruker) was used to confirm glioma maturity. The indication for PET guided CED are mature glioma (Fig. 3A) that are 2 to 4 mm in diameter in the right striatum by MR imaging (T2WI). Only mice bearing glioma between 2 and 4 mm in diameter were used to image [^{18}F]-**1** delivery. Orthotopic glioma that are larger than 4 mm in mice were acutely lethal, while glioma that were less than 2 mm generally did not elicit symptoms (and did not indicate a need for scanning) in mice.

Five representive mice (Figs. 3A–C and 4A) are used to compare CED and systemic delivery. Two mice were correctly infused with [^{18}F]-**1** by CED (Fig. 3Ai and ii, 3Bi and ii, 3Ci and ii, 4Aii). A third mouse (Fig. 3Aiii, 3Biii, and 4Aiii) was infused with [^{18}F]-**1** through CED after movement had translated into a dislodged cannula immediately prior to CED, so that [^{18}F]-**1** was misdelivered and glioma-CED delivery was not achieved. Two more mice (Fig. 3Aiv and v, and 4iv and v) were injected with [^{18}F]-**1** through the tail vein (systemic intravenous delivery) so that CED and systemic delivery of compound 1 could be compared. Mice were imaged over a 3-hour period.

Aligning PET/CT and MR for CED quantitation

Murine orthotopic glioma are not well visualized by micro CT, making PET/MR necessary for imaging the delivery of [^{18}F]-**1** to CNS neoplasms. Real-time PET/CT and pre-acquired MR DICOM from separate 7-Tesla MR (Bruker) and Inveon PET/CT were aligned to generate PET/MR data. The skull, orbits, olfactory bulb, and incisors provide accurate fiducial markers for alignment. Examples of correctly aligned PET/CT/MR are shown in Fig. 3B. Horizontal MR horizontal sections are shown superimposed onto CT maximum intensity projections.

Qualitative imaging delivery of 1 by ^{18}F-PET/MR

PET/MR allows observation of the exact advantage between CED and systemic drug delivery. A 6 μL volume containing 50 μmol/L of [^{18}F]-**1** (300 pmols, 0.35 μg) was administered via CED (60 minutes at 0.1 μL/minute) through a cannula placed for CED in glioma (see video S3–S5 in supplementary information). Figure 3Ci and ii shows prompt and accurate CED of [^{18}F]-**1** to glioma by ^{18}F-PET.

PET imaging can immediately indicate a dislodged or improperly placed cannula, where movement translates into a dislodged cannula prior to CED. Figure 3Ciii and Fig. 4Aiii illustrate the highly personalized nature of CED and highlight a need for imaging in CED. Glioma occupy different volumes and have

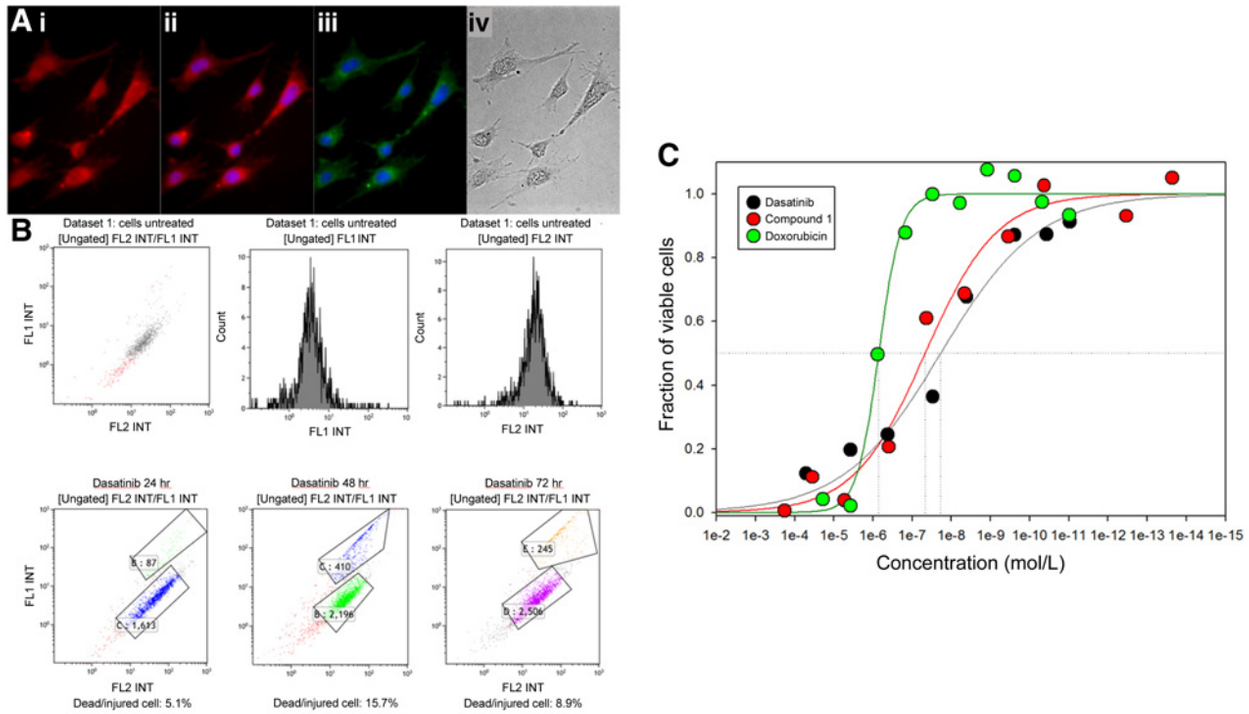

Figure 2.

In vitro studies show that compound **1** is fluorescent and can reduce mouse brainstem glioma cell proliferation. **A,** [^{19}F]-**1** is fluorescent in mBSG culture. (**i**) Fluorescence imaging of mBSG co-incubated with [^{18}F]-**1** shows fluorescence localization to glioma cells (15 minutes incubation). (**ii**) Combined [^{19}F]-**1** fluorescence (red) and DAPI (blue) nuclei staining show similar distribution as (**iii**) cell mask plasma membrane stain (green)/DAPI (blue). (**iv**) Trans illumination. **B,** [^{19}F]-**1** shows similar activity cytotoxicity to unmodified dasatinib when delivered against murine brainstem glioma cells. Cells originally isolated from mouse DIPG induced by PDGF-B overexpression and p53 loss were cultured as adherent monolayers, and treated with 100 nmol/L of **1** or vehicle (DMEM media) at varying time points. Cell viability was assessed with Live/Dead C^{12} Resazurin, SYTOX viability assay. First row represents cells treated with vehicle alone. Second row represent cells treated with **1** at 24, 48, and 72 hours. FL1–Resazurin channel (viability); FL2–Cy3 fluorescence. **C,** Dasatinib and doxorubicin were determined to have the lowest mBSG IC_{50} values in a panel of tested drugs (Supplementary Figs. S4 and S5). IC_{50} data compiled from average cell viability data on pontine glioma cell lines from 6, 96-well plates performed over a 3-week period compiled from ATP-dependent luminescent cell viability, cell-permeant calcein AM, and MTS cell proliferation assays. R^2 values = 0.972 for dasatinib, 0.975 for [^{19}F]-**1**, and 0.987 for doxorubicin. IC_{50} values (and SEM) are dasatinib, 19 ± 20 nmol/L; PET/FL compound **1**, 46 ± 30 nmol/L; and doxorubicin 710 ± 120 nmol/L.

different-drug retention properties, making CED planning highly personalized. Nevertheless, CED delivery is still superior to intravenous delivery in delivering high concentrations of [^{18}F]-**1** to glioma. This experiment is shown in Fig. 4 (and video S6–S7 in supplementary information) where, mice bearing glioma are injected with the same physical and radioactive quantities of [^{18}F]-**1**, by CED and intravenously through the tail vein. Following CED, **1** is cleared through the gastrointestinal system. This is observed at late timepoint PET imaging, and is verified by *ex vivo* fluorescence imaging (Fig. 4B) in mice that were sacrificed immediately following PET scanning.

Quantiative imaging of delivery of 1 by ^{18}F-PET/MR

[^{18}F]-**1** CED delivery to glioma were calculated using standardized uptake values (SUV) from dynamic PET imaging regions of interest (ROIs). SUVs were placed over glioma, and over contralateral (control) volumes (Fig. 5).

ROI volumes (Fig. 5A) allow for SUV-based quanitiation of the delivery and clearance of [^{18}F]-**1** (Fig. 5B) by CED and intravenous routes of drug delivery. CED is superior to systemic injections of [^{18}F]-**1** in the CNS and glioma. Intravenous delivery results in a smaller fraction of drug delivered to the intracranial glioma site (Fig. 5, Table 1). CED bypasses the blood brain barrier, and is 13,000 times more effective than systemic injection at delivering dasatinib to a glioma. In the case of CED, shown in Fig. 5Aii, maximal glioma concentration occurs at 135 minutes into the PET scan, (22 μmol/L, 117 minutes postCED). [^{18}F]-**1** continues to accumulate at glioma following a 60-minute CED (CED is complete at 75 minutes vs. PET scan start). Continued accumulation of [^{18}F]-**1** at glioma ROI following the completion of CED indicates continued flow from the site of CED into the glioma. This may be due to inexact CED cannula-glioma alignment, or nonuniform convection through a heterogeneous glioma. Fifty percent of [^{18}F]-**1** clears approximately 36 minutes following maximum drug accumulation ($t_{1/2}$). These delivery properties are observable with [^{18}F]-**1**, but would not be visible in drugs that do not have a PET label.

CED histology and assessment of safety

Orthotopic glioma bearing tissues were collected and evaluated by immunohistochemical staining (Supplementary Figs. S2 and S3). Long-term neurotoxicity is not detected in histology on tissue of naive animals who recieve CED delivered [^{18}F]-**1** and are allowed to recover for 30 days (Supplementary Fig. S4).

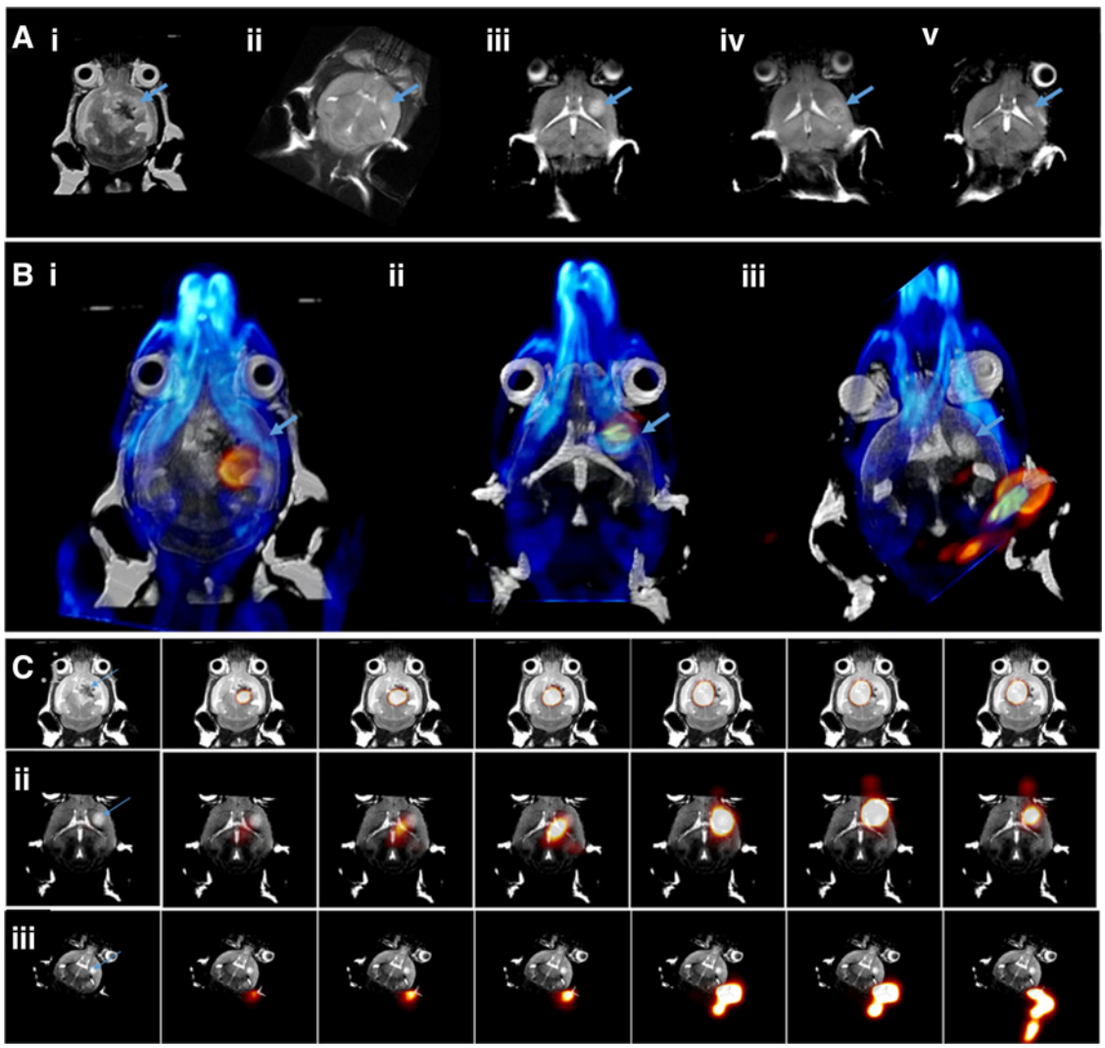

Figure 3.

MR (gray) imaging of orthotopic glioma and PET (red)/CT (blue)/MR imaging of dynamic CED of [^{18}F]-**1**. **A,** MR (T2 weighted imaging) of mature glioma bearing mice receiving [^{18}F]-**1** by CED (**i**, **ii**, and **iii**) and tail vein (**iv**, **v**). **B,** PET/CT/MR overlay. Early time point imaging of a 6 μL, 15 μCi dose of [^{18}F]-**1** by CED at 50 μmol/L initial concentration. **C,** PET/MR dynamic imaging of accurate [^{18}F]-**1** CED delivery [(**i**) 0, 5, 7, 9, 35, 40, and 60 minutes, see video S2 in supplementary information], and (**ii**) 0, 25, 30, 35 125, 140, and 160 minutes. (**iii**) Images of an incorrectly delivered dose of [^{18}F]-**1** at 0, 20, 25, 30, 125, 140, and 160 minutes. Blue arrows, location of glioma. Times are versus beginning of PET scan (0 minute), CED was started 17 minutes into the PET scan.

Discussion

The synthesis and ^{18}F-radiolabeling of compound **1**, a nanomolar chemotherapeutic with a mechanism of action that is similar to dasatinib, is described. Methodology for imaging its delivery to orthotopic glioma systemically and by CED is also described. Following delivery, the PET imaging of [^{18}F]-**1** allows for real time quantitation of drug retention and clearance from the delivery site. Acquired PET data provide information relevant to CED infusion and redosing, so that steady states of drug can be maintained at glioma, in practice.

New methods for delivering drugs to neurological disorders

Rates of drug delivery and clearance to/from glioma can vary with catheter positioning, delivery technique, and even internally, between CED studies (38, 39). The murine model, and the PET and FL visibility of [^{18}F]-**1** is applied to CED in this report, but it should be noted that these methodologies should have utility in quantitating or contrasting drug delivery in other popular new methods, such as focused ultrasound (FU) or mannitol assisted delivery (1, 16). The described methodology should have additional utility in advanced, combined drug delivery efforts, such as FU-CED, a promising delivery combination.

Limits of PET and the need for fluorescence in accurately imaging drug clearance

^{18}F-PET is currently less useful at submicron spatial resolutions. A PET tracer cannot be used to observe extracellular membrane penetration of a drug in intact cells, for example, [^{18}F]-**1** PET

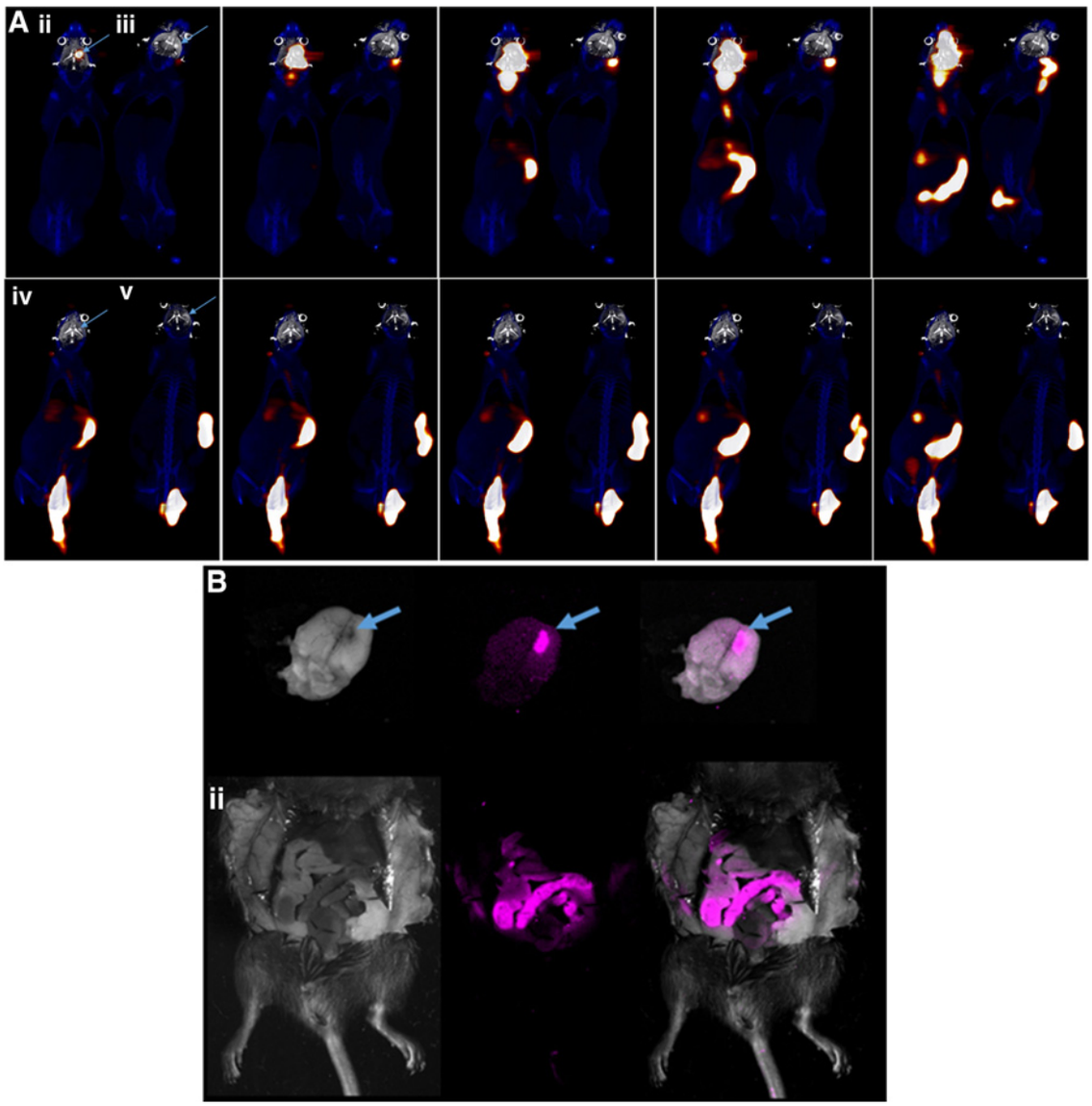

Figure 4.

PET(red)/CT(blue)/MR(gray)/Fluorescence (pink) imaging show delivery and clearance of [^{18}F]-**1** to glioma by CED and tail vein injection. **A,** [^{18}F]-**1** delivery by CED (**ii**, **iii**) and tail vein (**iv**, **v**) at similar concentrations. Blue arrows, glioma location. Correct CED delivery to glioma (**ii**) is imaged alongside incorrect delivery (**iii**) at 15, 25, 40, 70, and 160 minutes (vs. start of PET scan, see video S3–S5 in supplementary information). [^{18}F]-**1** misdelivery as well as clearance is clearly visible by PET. In contrast, accumulation in glioma is not seen in systemically injected mice at time points of 60, 80, 90, 110, and 160 minutes postinjection (see video S6–7 in supplementary information). A higher concentration of [^{18}F]-**1** is delivered to glioma via CED versus systemic injection. Times are versus beginning of PET scan (0 minute), CED was started 17 minutes into the PET scan. **B,** Immediate *ex vivo* fluorescence analysis of [^{18}F]-**1** delivered by CED. To verify the general PET biodistribution of [^{18}F]-**1**, mice receiving [^{18}F]-**1** by CED were dissected following the PET scan and analyzed in a Bruker xtreme optical animal imaging system. (left to right) Bright field image, fluorescence, and merged image dissection confirm distribution of [^{18}F]-**1** at (**i**) the CED site and (**ii**) clearance through the intestine. Fluorescence data corroborate late image PET data in **A**.

cannot be used to observe movement from the extracellular space into a cell's cytosol. This can be a problem when comparing systemic and CED delivery. The spatial resolution of ^{18}F-PET makes it difficult to distinguish between drug that is present in the brain capillaries (on the blood side of the blood brain barrier) and that which has penetrated the parenchyma. Because CED delivers a drug to the intratumoral space directly (2), PET and ROI-based quantitation of systemic deliveries may overestimate the presence of drug that is delivered systemically to orthotopic glioma relative versus CED.

Fluorescence imaging is a higher resolution technique, which is used to resolve drug transport at the cellular level, for example, transport into the cytosol or into subcellular organelles *in vitro* or *ex vivo* (histology). [^{18}F]-**1** contains a fluorophore for *in vitro*/*ex vivo* confirmative imaging of drug delivery (fluorescence guided surgery or histology). In the design of [^{18}F]-**1**, we choose to

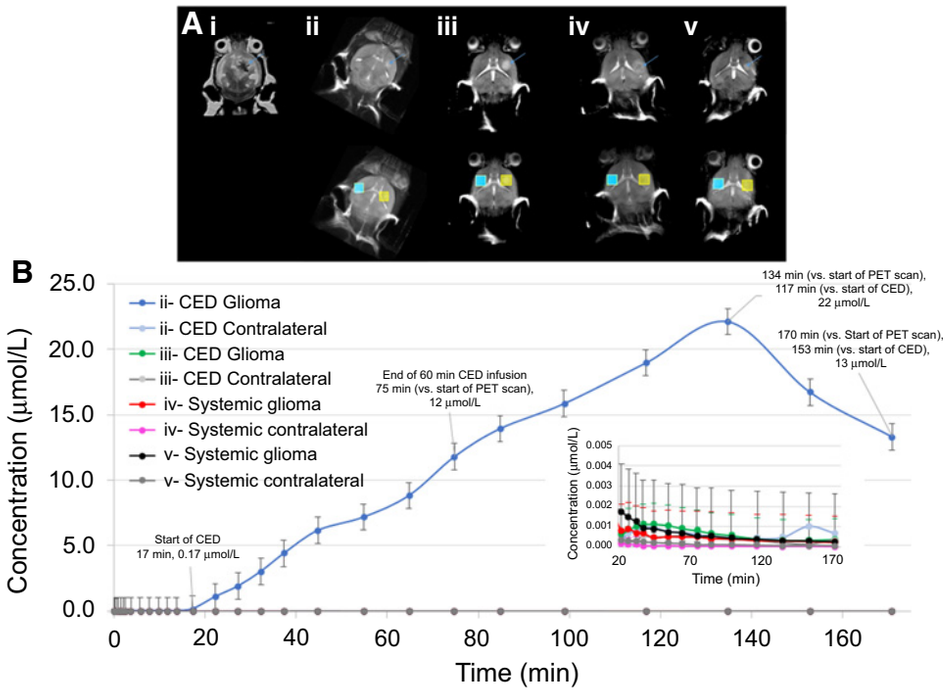

Figure 5.
Quantifying glioma delivery and clearance of [^{18}F]-**1**. **A,** Regions of interest (cubic, 2 mm^3) placed directly over glioma (yellow) and over contralateral volumes (cyan) in PET/CT/MR to quantitate the accumulation of [^{18}F]-**1** received by mice via CED (**ii**), incorrect CED delivery (**iii**), or systemically by tail vein (**iv**, **v**). Blue arrow, location of gliomas. **B,** Quantitation of drug accumulation and clearance of [^{18}F]-**1**. The PET scan was started at 0 minutes, CED infusion was initiated at 17 minutes. Regions of interest (ROI) were converted to concentrations (obtained via by placing equivolume ROI over cannula filled with [^{18}F]-**1**, prior to [^{18}F]-**1** delivery, calibrated at 50 μmol/L). CED delivery of [^{18}F]-**1** to a glioma accumulates maximally in mouse (**ii**) at 135 minutes (117 minutes postCED, note continued accumulation in glioma postCED indicate continued convection of drug from cannula into glioma ROI; ii). Incorrect CED placement (**iii**) and systemic injection (**iv**, **v**) only deliver a fraction of [^{18}F]-**1** to a glioma versus CED (**ii**).

combine ^{18}F with a cyanine fluorophore [^{18}F]-**1**, so that it is structurally related to indocyanine green (ICG), a fluorophore that has limited toxicity and is approved for clinical use.

[^{18}F]-**1** can be used by itself, as a stand-alone theranostic agent, or within a mixture with dasatinib. In a delivered mixture, it is important to consider that [^{18}F]-**1** and dasatinib may distribute at different rates.

This work sets precedent for transforming an alkyltrifluoroborate ^{18}F-trap onto other amine bearing chemotherapeutics for identifying drugs that have superior retention properties at glioma, without the need to rely on nontherapeutic surrogate tracers.

A need to immediately diagnose missed drug delivery

The need to immediately identify missed drug delivery is of paramount importance. Without the ability to image drug delivery, we currently assume that agents are delivered to glioma at adequate doses. This assumption is valid until a clinical indication presents to suggest otherwise (glioma growth, lack of volume reduction). This is unacceptable in glioma, as a tumor must progress significantly before drug misdelivery is realized. Image guided drug delivery allows the evaluation of proper drug delivery to the CNS by PET. Chemotherapeutics that allow for simultaneous imaging allow the observation of drug delivery in real time, so that inadequate intervention can be immediately corrected. Additionally, image guided delivery allows the characterization of insufficient or heterogeneous drug delivery to a glioma and the confirmation of comprehensive, saturating drug distribution to the margins of a diffuse glioma. Therapeutic imaging agents like [^{18}F]-**1** allow us to correlate therapy with imaging to generate guidelines for proper, missed, or insufficient *in vivo* drug delivery. Indeed, there is a need for intraoperative imaging in drug delivery, which has been shown to allow greater clinical efficacy when using CED in patients by direct monitoring and control of local delivery (40, 41).

Conclusion

We report the synthesis of [^{18}F]-**1,** a ^{18}F-PET/fluorescent derivative of dasatinib that is delivered to murine glioma by CED. PET

Table 1. ROI maximum intensities and maximum accumulation times of [^{18}F]-1 glioma accumulation and clearance in Fig. 5 glioma bearing mice

Mouse	Injection	Time of maximum accumulation at glioma (vs. CED start) (min)	Measured concentration maximum at glioma (nmol/L)	Time of maximum contralateral signal (vs. CED start) (min)	Concentration at contralateral ROI (Molar)	Fold more effective CED is versus mis- or systemic delivery	Ratio of CED delivery versus contralateral ROI
ii	CED	117	22,000 nmol/L	138	1.1 nmol/L		20,000
iii	CED-misdelivered	33	1.1 nmol/L		0.55 nmol/L	20,000×	
iv	Systemic (tail vein)		1.1 nmol/L		0.22 nmol/L	20,000×	
v	Systemic (tail vein)		1.65 nmol/L		0.55 nmol/L	13,333×	

NOTE: The tables shows that the CED delivery of [^{18}F]-**1** to a glioma accumulates maximally at glioma in (**b**), 117 minutes following a 60 minute-CED infusion (135 minutes vs. start of PET scan). Incorrect CED (**c**) and systemic injection (**d, e**) only deliver a fraction of [^{18}F]-**1** to a glioma.

and fluorescence imaging is used to compare CED with systemic delivery, quantitate drug clearance from glioma, and immediately diagnose missed delivery.

Disclosure of Potential Conflicts of Interest

M.M. Souweidane has received speakers bureau honoraria from and is a consultant/advisory board member for Aesculap. No potential conflicts of interest were disclosed by the other authors.

Authors' Contributions

Conception and design: M. Wang, H. Kommidi, U. Tosi, Z. Zhou, R. Singh, B. Law, R. Ting, M.M. Souweidane
Development of methodology: M. Wang, H. Kommidi, U. Tosi, Z. Zhou, R. Singh, R. Ting, M.M. Souweidane
Acquisition of data (provided animals, acquired and managed patients, provided facilities, etc.): M. Wang, U. Tosi, H. Guo, Z. Zhou, M.E. Schweitzer, L.Y. Wu, S. Hou, R. Ting
Analysis and interpretation of data (e.g., statistical analysis, biostatistics, computational analysis): M. Wang, H. Kommidi, U. Tosi, H. Guo, Z. Zhou, S. Hou, R. Ting, M.M. Souweidane
Writing, review, and/or revision of the manuscript: M. Wang, H. Kommidi, U. Tosi, H. Guo, Z. Zhou, M.E. Schweitzer, L.Y. Wu, R. Singh, R. Ting, M.M. Souweidane
Administrative, technical, or material support (i.e., reporting or organizing data, constructing databases): B. Law, R. Ting, M.M. Souweidane
Study supervision: R. Ting, M.M. Souweidane

Acknowledgments

The project is supported by grants from the National Institute of Biomedical Imaging and Bioengineering (K99/R00EB013904, R. Ting), the Alex Lemonade Stand Foundation for Childhood Cancer (M. Souweidane), the Alex Lemonade Stand Foundation Pediatric Oncology Student Training Program (U. Tosi), the Matthew Larson Foundation for Pediatric Brain Tumors Research Grant (R. Ting, M. Souweidane, and B. Law), and the St. Baldrick's Summer Fellow Grant (M. Wang).

The costs of publication of this article were defrayed in part by the payment of page charges. This article must therefore be hereby marked *advertisement* in accordance with 18 U.S.C. Section 1734 solely to indicate this fact.

Received May 11, 2017; revised August 21, 2017; accepted September 18, 2017; published OnlineFirst October 4, 2017.

References

1. Parrish KE, Sarkaria JN, Elmquist WF. Improving drug delivery to primary and metastatic brain tumors: strategies to overcome the blood-brain barrier. Clin Pharmacol Ther 2015;97:336–46.
2. Bobo RH, Laske DW, Akbasak A, Morrison PF, Dedrick RL, Oldfield EH. Convection-enhanced delivery of macromolecules in the brain. Proc Natl Acad Sci U S A 1994;91:2076–80.
3. Luther N, Zhou Z, Zanzonico P, Cheung NK, Humm J, Edgar MA, et al. The potential of theragnostic (1)(2)(4)I-8H9 convection-enhanced delivery in diffuse intrinsic pontine glioma. Neuro Oncol 2014;16:800–6.
4. Zhou Z, Singh R, Souweidane MM. Convection-enhanced delivery for diffuse intrinsic pontine glioma treatment. Curr Neuropharmacol 2017; 15:116–28.
5. Zhou Z, Ho SL, Singh R, Pisapia DJ, Souweidane MM. Toxicity evaluation of convection-enhanced delivery of small-molecule kinase inhibitors in naive mouse brainstem. Childs Nerv Syst 2015;31:557–62.
6. Cawthorne C, Burrows N, Gieling RG, Morrow CJ, Forster D, Gregory J, et al. [18F]-FLT positron emission tomography can be used to image the response of sensitive tumors to PI3-kinase inhibition with the novel agent GDC-0941. Mol Cancer Ther 2013;12:819–28.
7. Goldberg L, Ocherashvilli A, Daniels D, Last D, Cohen ZR, Tamar G, et al. Salirasib (farnesyl thiosalicylic acid) for brain tumor treatment: a convection-enhanced drug delivery study in rats. Mol Cancer Ther 2008;7:3609–16.
8. Hardy PA, Keeley D, Schorn G, Forman E, Ai Y, Venugopalan R, et al. Convection enhanced delivery of different molecular weight tracers of gadolinium-tagged polylysine. J Neurosci Methods 2013;219:169–75.
9. Asthagiri AR, Walbridge S, Heiss JD, Lonser RR. Effect of concentration on the accuracy of convective imaging distribution of a gadolinium-based surrogate tracer. J Neurosurg 2011;115:467–73.
10. Takahashi M, Tsutsui H, Murayama C, Miyazawa T, Fritz-Zieroth B. Neurotoxicity of gadolinium contrast agents for magnetic resonance imaging in rats with osmotically disrupted blood-brain barrier. Magn Reson Imaging 1996;14:619–23.
11. Feng X, Xia Q, Yuan L, Yang X, Wang K. Impaired mitochondrial function and oxidative stress in rat cortical neurons: implications for gadolinium-induced neurotoxicity. Neurotoxicology 2010;31:391–8.
12. Junck L, Marshall WH. Neurotoxicity of radiological contrast agents. Ann Neurol 1983;13:469–84.
13. Taylor H, Barua N, Bienemann A, Wyatt M, Castrique E, Foster R, et al. Clearance and toxicity of recombinant methionyl human glial cell line-derived neurotrophic factor (r-metHu GDNF) following acute convection-enhanced delivery into the striatum. PLoS One 2013;8:e56186.
14. Halvorson KG, Barton KL, Schroeder K, Misuraca KL, Hoeman C, Chung A, et al. A high-throughput in vitro drug screen in a genetically engineered mouse model of diffuse intrinsic pontine glioma identifies BMS-754807 as a promising therapeutic agent. PLoS One 2015;10: e0118926.
15. Tsien RY. Imagining imaging's future. Nat Rev Mol Cell Biol 2003;Suppl: SS16–21.
16. Tosi U, Marnell CS, Chang R, Cho WC, Ting R, Maachani UB, et al. Advances in molecular imaging of locally delivered targeted therapeutics for central nervous system tumors. Int J Mol Sci 2017;18:351–69.
17. Zhou Z, Luther N, Ibrahim GM, Hawkins C, Vibhakar R, Handler MH, et al. B7-H3, a potential therapeutic target, is expressed in diffuse intrinsic pontine glioma. J Neurooncol 2013;111:257–64.
18. Korashy HM, Rahman AF, Kassem MG. Dasatinib. Profiles Drug Subst Excip Relat Methodol 2014;39:205–37.
19. Veach DR, Namavari M, Pillarsetty N, Santos EB, Beresten-Kochetkov T, Lambek C, et al. Synthesis and biological evaluation of a fluorine-18 derivative of dasatinib. J Med Chem 2007;50:5853–7.
20. Dunphy MP, Zanzonico P, Veach D, Somwar R, Pillarsetty N, Lewis J, et al. Dosimetry of 18F-labeled tyrosine kinase inhibitor SKI-249380, a dasatinib-tracer for PET imaging. Mol Imaging Biol 2012;14:25–31.
21. Benezra M, Hambardzumyan D, Penate-Medina O, Veach DR, Pillarsetty N, Smith-Jones P, et al. Fluorine-labeled dasatinib nanoformulations as targeted molecular imaging probes in a PDGFB-driven murine glioblastoma model. Neoplasia 2012;14:1132–43.
22. Broniscer A, Baker SD, Wetmore C, Pai Panandiker AS, Huang J, Davidoff AM, et al. Phase I trial, pharmacokinetics, and pharmacodynamics of vandetanib and dasatinib in children with newly diagnosed diffuse intrinsic pontine glioma. Clin Cancer Res 2013;19:3050–8.
23. Wang RE, Liu T, Wang Y, Cao Y, Du J, Luo X, et al. An immunosuppressive antibody-drug conjugate. J Am Chem Soc 2015;137:3229–32.
24. Liu Z, Chao D, Li Y, Ting R, Oh J, Perrin DM. From minutes to years: predicting organotrifluoroborate solvolysis rates. Chemistry 2015;21: 3924–8.
25. Ting R, Harwig CW, Lo J, Li Y, Adam MJ, Ruth TJ, et al. Substituent effects on aryltrifluoroborate solvolysis in water: implications for Suzuki-Miyaura coupling and the design of stable (18)F-labeled aryltrifluoroborates for use in PET imaging. J Org Chem 2008;73:4662–70.
26. Misuraca KL, Cordero FJ, Becher OJ. Pre-clinical models of diffuse intrinsic pontine glioma. Front Oncol 2015;5:172.
27. Hambardzumyan D, Amankulor NM, Helmy KY, Becher OJ, Holland EC. Modeling adult gliomas using RCAS/t-va technology. Transl Oncol 2009;2:89–95.
28. Tokarski JS, Newitt JA, Chang CY, Cheng JD, Wittekind M, Kiefer SE, et al. The structure of dasatinib (BMS-354825) bound to activated ABL kinase

domain elucidates its inhibitory activity against imatinib-resistant ABL mutants. Cancer Res 2006;66:5790–7.
29. Vetter ML, Zhang ZJ, Liu S, Wang JH, Cho H, Zhang JM, et al. Fluorescent visualization of Src by using dasatinib-BODIPY. ChemBioChem 2014; 15:1317–24.
30. Ting R, Aguilera TA, Crisp JL, Hall DJ, Eckelman WC, Vera DR, et al. Fast 18F labeling of a near-infrared fluorophore enables positron emission tomography and optical imaging of sentinel lymph nodes. Bioconjug Chem 2010;21:1811–9.
31. Ting R, Adam MJ, Ruth TJ, Perrin DM. Arylfluoroborates and alkylfluorosilicates as potential PET imaging agents: high-yielding aqueous biomolecular 18F-labeling. J Am Chem Soc 2005;127: 13094–5.
32. Liu Z, Pourghiasian M, Radtke MA, Lau J, Pan J, Dias GM, et al. An organotrifluoroborate for broadly applicable one-step F-labeling. Angew Chem Int Ed Engl 2014;53:11876–80.
33. Perrin DM. [18F]-Organotrifluoroborates as radioprosthetic groups for PET imaging: from design principles to preclinical applications. Acc Chem Res 2016;49:1333–43.
34. Rodriguez EA, Wang Y, Crisp JL, Vera DR, Tsien RY, Ting R. New dioxaborolane chemistry enables [18F]-positron-emitting, fluorescent [18F]-multimodality biomolecule generation from the solid phase. Bioconjugate Chem 2016;27:1390–9.
35. Araujo J, Logothetis C. Dasatinib: a potent SRC inhibitor in clinical development for the treatment of solid tumors. Cancer Treat Rev 2010; 36:492–500.
36. Dalgç CT, Kaymaz BT, Özkan MC, Dalmzrak A, Şahin F, Saydam G. Investigating the role of JAK/STAT pathway on dasatinib-induced apoptosis for CML cell model K562. Clin Lymphoma Myeloma Leuk 2015; 15 Suppl:S161–6.
37. Lu H, Wang L, Gao W, Meng J, Dai B, Wu S, et al. IGFBP2/FAK pathway is causally associated with dasatinib resistance in non-small cell lung cancer cells. Mol Cancer Ther 2013;12:2864–73.
38. Allard E, Passirani C, Benoit JP. Convection-enhanced delivery of nanocarriers for the treatment of brain tumors. Biomaterials 2009; 30:2302–18.
39. Morrison PF, Laske DW, Bobo H, Oldfield EH, Dedrick RL. High-flow microinfusion: tissue penetration and pharmacodynamics. Am J Physiol 1994;266(1 Pt 2):R292–305.
40. Croteau D, Walbridge S, Morrison PF, Butman JA, Vortmeyer AO, Johnson D, et al. Real-time in vivo imaging of the convective distribution of a low-molecular-weight tracer. J Neurosurg 2005;102:90–7.
41. Saito R, Krauze MT, Bringas JR, Noble C, McKnight TR, Jackson P, et al. Gadolinium-loaded liposomes allow for real-time magnetic resonance imaging of convection-enhanced delivery in the primate brain. Exp Neurol 2005;196:381–9.